Supporting Information

$[Sn_8]^{6-}$-Bridged Mixed-Valence Zn^I/Zn^{II} in $\{[K_2ZnSn_8(ZnMes)]_2\}^{4-}$ Inverse Sandwich-Type Cluster Supported by a Zn^I-Zn^I Bond

Hong-Lei Xu, Nikolay V. Tkachenko, Alvaro Muñoz-Castro, Alexander I. Boldyrev,* and Zhong-Ming Sun*

anie_202102578_sm_miscellaneous_information.pdf

Table of Contents

Section 1: Experimental Procedures

All manipulations and reactions were performed under a nitrogen atmosphere using standard Schlenk or glovebox techniques. Ethylenediamine (en) (Aldrich, 99%) and DMF (Aldrich, 99.8%) were freshly distilled by CaH_2 prior to use. Toluene (Aldrich, 99.8%) was distilled from sodium/benzophenone under nitrogen and stored under nitrogen. 2,2,2-crypt (4,7,13,16,21,24-Hexaoxa-1,10-diazabicyclo (8.8.8) hexacosane, purchased from Sigma-Aldrich, 98%) was dried in vacuum for 20 h prior to use. The ternary mixture with a nominal composition of "K_4ZnSn_4" was synthesized by heating a stoichiometric mixture of the elements (K: +99 %, Sn: 99.99 %, Zn: 99 % all from Aladdin) at a rate of 100 °C per hour to 800 °C and keeping it for 10 hours in sealed niobium containers closed in evacuated quartz ampules. The furnace was slowly cooled to room temperature at a rate of 100 °C per hour. $ZnMes_2$ was synthesized according to the reported literatures. [1]

Synthesis of [K(2,2,2-crypt)]$_4${[K$_2$ZnSn$_8$(ZnMes)]$_2$} (1):
The phase of the nominal composition of "K_4ZnSn_4" (100 mg, 0.144 mmol) and 2.2.2-crypt (100 mg, 0.265 mmol) were dissolved in en (2.5 mL) inside a glovebox. After stirring for 5 min, the resulting brown-red solution was filtered onto another vial with a 0.5 mL toluene solution of $ZnMes_2$ (35 mg, 0.115 mmol) and stirring for a further three hours at room temperature. The resulting brown-red solution was filtered through glass wool and carefully layered by toluene (3 mL) to allow for crystallization. After 20 days, dark-red plate crystals were obtained in the test tube in approximately 21% yield (based on loaded starting material $ZnMes_2$).

X-ray Diffraction:
Suitable single crystals were selected for X-ray diffraction analyses. Crystallographic data were collected on Rigaku XtalAB Pro MM007 DW diffractometer with graphite monochromated Cu Kα radiation (λ = 1.54184 Å). Structure was solved using direct methods and then refined using SHELXL-2014 and Olex2 [2-4] to convergence, in which all the non-hydrogen atoms were refined anisotropically. All hydrogen atoms of the organic molecule were placed by geometrical considerations and were added to the structure factor calculation. We used the PLATON SQUEEZE procedure [5] to remove the solvent molecules which could not be modeled properly. Because of the absorption effects, we carefully treated the data by means of the absorption correction to reduce the residual density close to the metal atoms Sn and Zn. Additionally, we refined the structure by using some requisite restrains of anisotropy, such as SIMU, DFIX, RIGU for the K-crypt fragments and omitting the most disagreeable reflections. The compound is very air and moisture sensitive in solution and the solid state which may be due to its high charges carrying four K(2,2,2-crypt) cations and four non-cryptated K-cations, and very thin crystals also make it not easy to obtain better data.

**Electrospray Ionization Mass Spectrometry (ESI-MS) Investigations:**
Negative ion mode ESI-MS of the DMF solution of the single crystal and reaction solution were measured on an LTQ linear ion trap spectrometer by Agilent Technologies ESI-TOF-MS (6230). The spray voltage was 5.48 kV and the capillary temperature was kept at 300 °C. The capillary voltage was 30 V. The sheath gas was 50 °C. The samples were prepared inside a glovebox and very rapidly transferred to the spectrometer in an airtight syringe by direct infusion with a Harvard syringe pump at 0.2 mL/min.

Energy Dispersive X-ray (EDX):
EDX analysis on the title clusters were performed using a scanning electron microscope (FE-SEM, JEOL JSM-7800F, Japan). Data acquisition was performed with an acceleration voltage of 15 kV and an accumulation time of 60 s.

Powder X-Ray Diffraction:
Powder X-ray diffraction (PXRD) data were collected on a Rigaku diffractometer using Cu Ka radiation (λ = 1.5418 Å). The sealed samples were scanned for every 0.01° increment over the Bragg angle range of 10−70°.
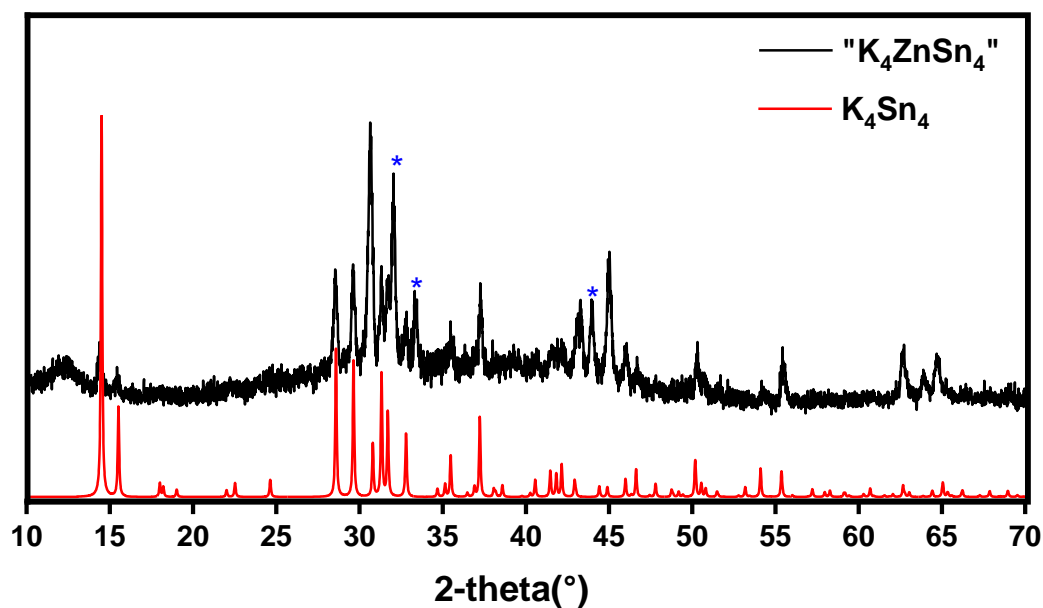
Figure S1. Measured powder X-ray diffraction (PXRD) pattern of "K_4ZnSn_4" (black) compared with the calculated pattern for K_4Sn_4 (red) [6]. The marked peaks are attributed to unknown compositions.

Quantum chemical methods:

Quantum chemical calculations (geometry optimization and frequency calculations) were performed using Gaussian 16 software package at the PBE0/Def2-TZVP level of theory. To account possible delocalization error of PBE0 functional, additional calculations were performed using CAM-B3LYP functional. To identify the chemical bonding of investigated species, we carried out adaptive natural density partitioning (AdNDP) analysis as implemented in the AdNDP 2.0 code. The ELF analysis and QTAIM atomic charge analysis were performed via MultiWFN software. In addition, the isosurface and cut-plane representation of the induced magnetic field (Bind) was obtained within the GIAO formalism at the relativistic ZORA-PBE0/TZ2P level of theory by using the ADF suite unraveling the long-range characteristics of the magnetic response. To analyze natural atomic charge distribution NBO7 software was used.[7]

Section 2: Crystallographic Supplementation
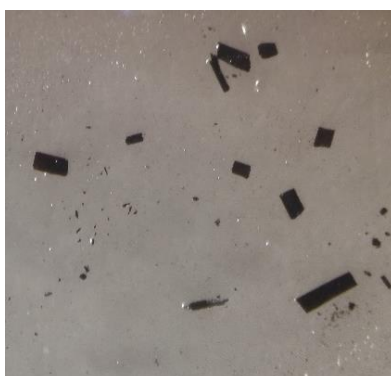
1

Figure S2. Crystals of $[K(2,2,2-crypt)]_4\{[K_2ZnSn_8(ZnMes)]_2\}$ (**1**) dispersed silicon oil.

**Table S1.** Crystal data and structure refinement .

| Identification code	**1**
Empirical formula	$C_{90}H_{166}N_8O_{24}K_8Zn_4Sn_{16}$
Formula weight	4217.62
Temperature/K	100
Crystal system	monoclinic
Space group	$P2_1/n$
a/Å	12.8576(2)
b/Å	25.4791(5)
c/Å	32.0844(5)
α/°	90
β/°	95.380(2)
γ/°	90
Volume/Å^3	10464.5(3)
Z	2
ρ_{calc}g/cm^3	1.339
μ/mm^{-1}	17.102
$F(000)$	4052.0
2Θ range for data collection/°	5.534 to 133.202
Reflections collected	42003
Data/restraints/parameters	18209/34/679
Goodness-of-fit on F^2	0.997
Final R indexes [I>=2σ (I)]	$R_1 = 0.0979$, $wR_2 = 0.2397$
Final R indexes [all data]	$R_1 = 0.1053$, $wR_2 = 0.2453$
Largest diff. peak/hole / e Å^{-3}	3.62/-2.32
CCDC	2051316

[a] $R_1 = \sum||F_o|-|F_c||/\sum|F_o|$; $wR_2 = \{\sum w[(F_o)^2-(F_c)^2]^2/\sum w[(F_o)^2]^2\}^{1/2}$
[b] $GooF = \{\sum w[(F_o)^2-(F_c)^2]^2/(n-p)\}^{1/2}$
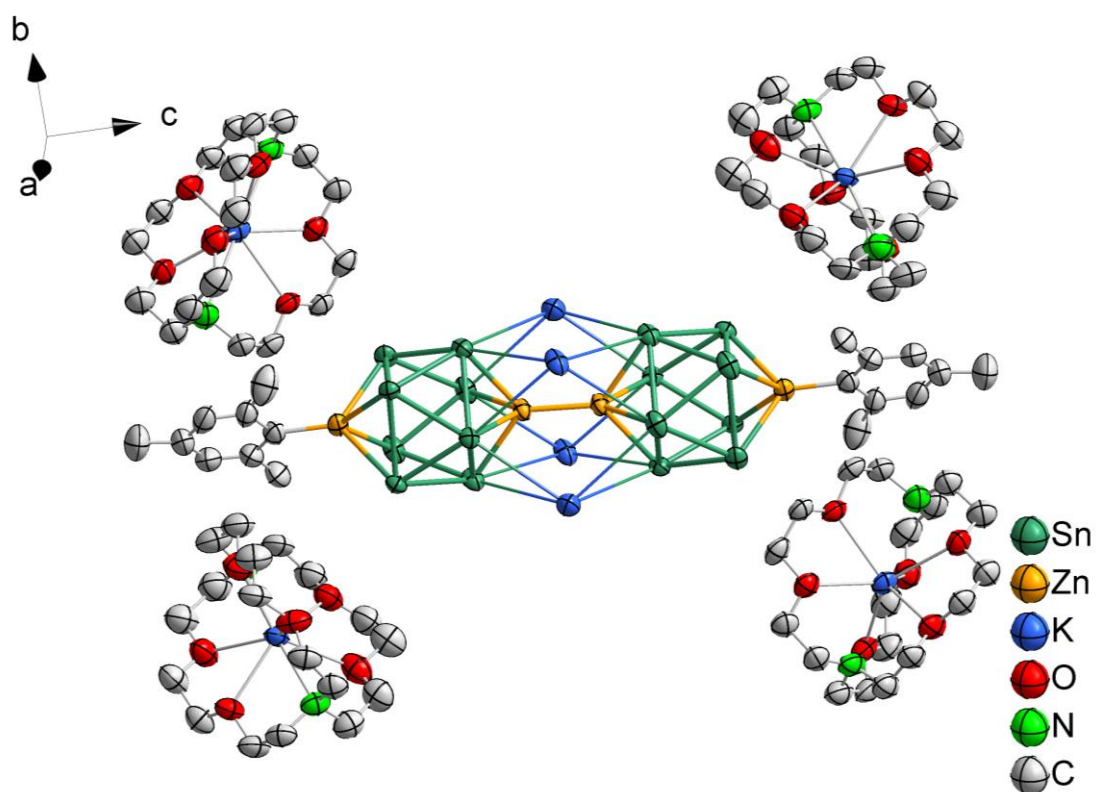
Figure S3. The molecular structure of **1** (thermal ellipsoids are drawn at 50% probability). The minor components are omitted for clarity.
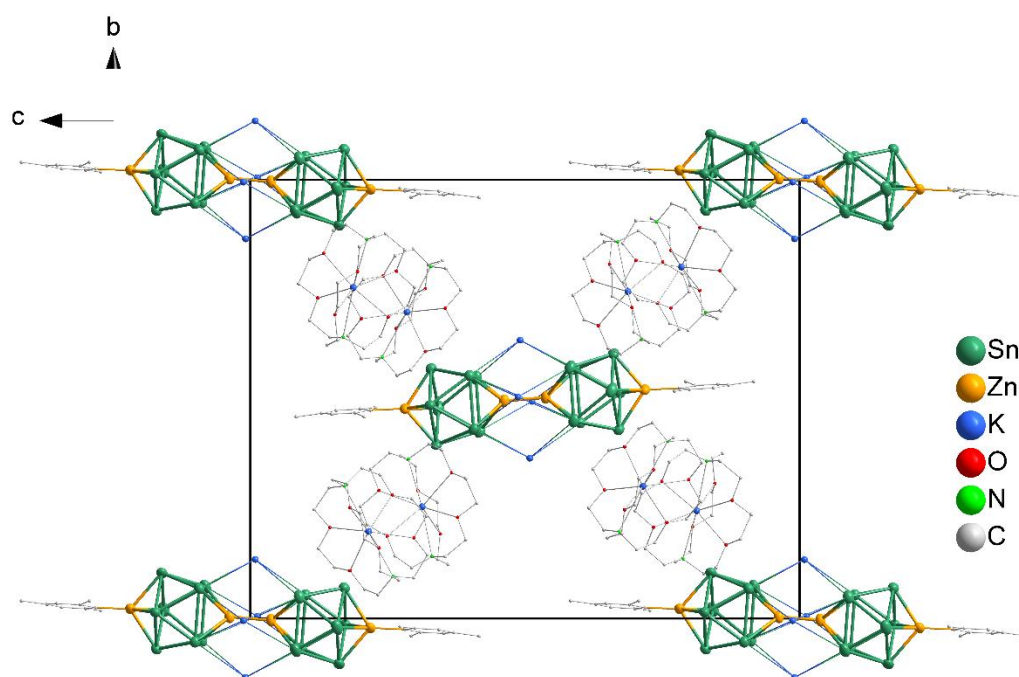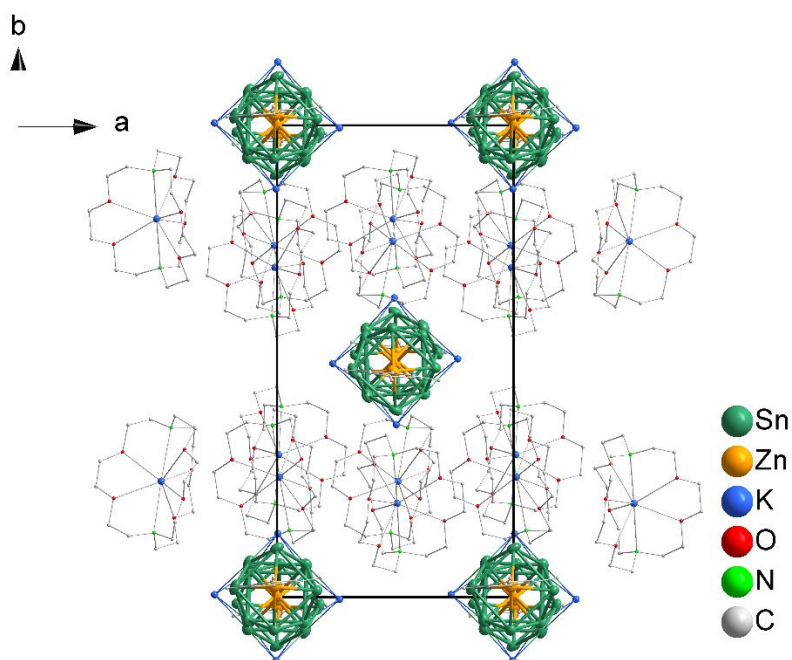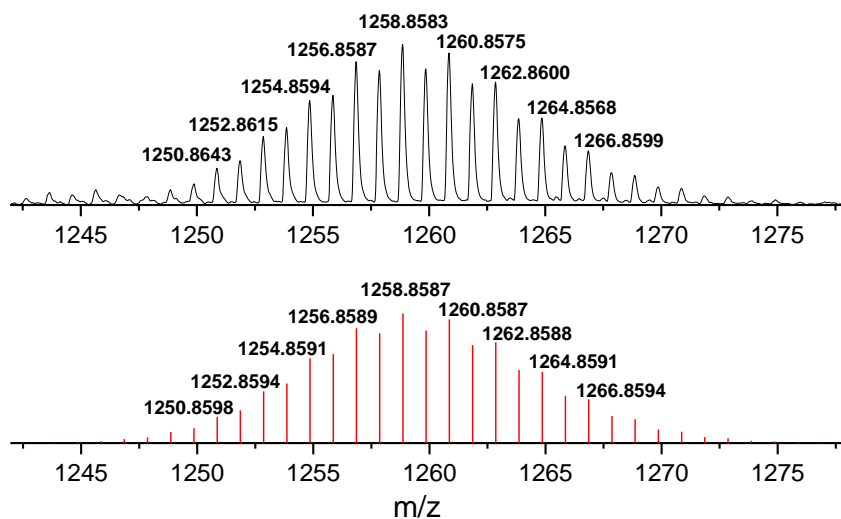
Figure S4. Unit cell of compound **1**. Minor components in the structure are omitted for clarity.
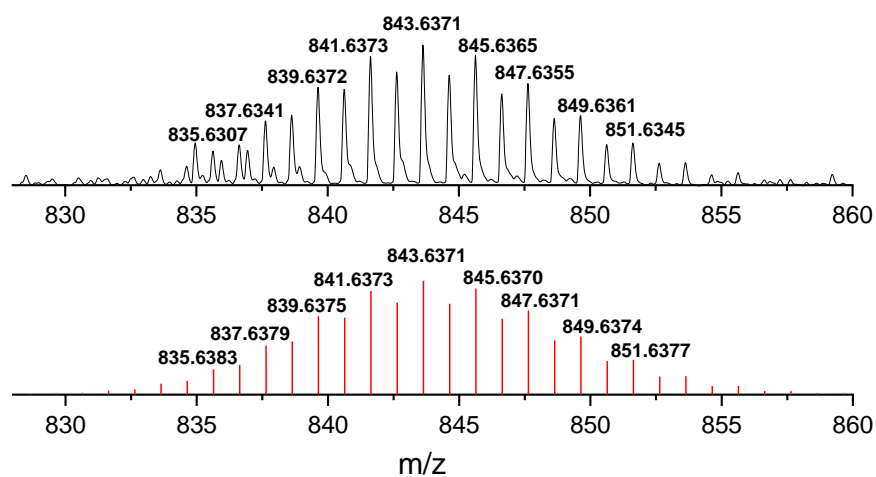
Section 3: ESI-MS Studies

Electrospray-ionization mass spectrometry (ESI-MS) on single crystals of **1** failed due to the fast decomposition during the experiments. Additionally, we also attempted to perform the ESI-MS of the reaction solution of "K_4ZnSn_4", $ZnMes_2$ and 2,2,2-crypt (Figure S5) under parallel experiments. Only several signals of small species were observed in the measured range due to {[Sn_4]}⁻ (m/z= 475.6058), {[$Sn_4(ZnMes)_2$]}⁻ (m/z= 843.6371), {[$KSn_4(ZnMes)_2$]}⁻ (m/z= 882.6004) and {[K(2,2,2-crypt)][$Sn_4(ZnMes)_2$]}⁻ (m/z= 1258.8583).
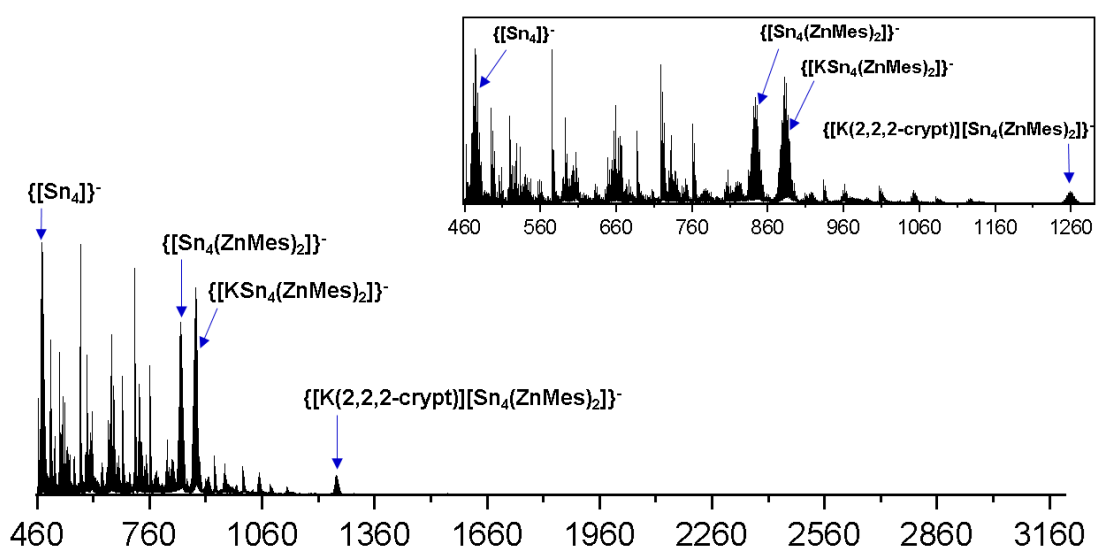
Figure S5. Overview ESI mass spectrum in negative ion mode recorded immediately upon injection of a fresh reaction solution of **1** in DMF.

6

1250.8643 **1252.8615** **1254.8594** **1256.8587** **1258.8583** **1260.8575** **1262.8600** **1264.8568** **1266.8599**

1250.8598 **1252.8594** **1254.8591** **1256.8589** **1258.8587** **1260.8587** **1262.8588** **1264.8591** **1266.8594**

m/z

Figure S6. Measured (top) and simulated (bottom) spectrum of the fragment $\{[K(2,2,2\text{-crypt})][Sn_4(ZnMes)_2]\}^-$.

835.6307 **837.6341** **839.6372** **841.6373** **843.6371** **845.6365** **847.6355** **849.6361** **851.6345**

835.6383 **837.6379** **839.6375** **841.6373** **843.6371** **845.6370** **847.6371** **849.6374** **851.6377**
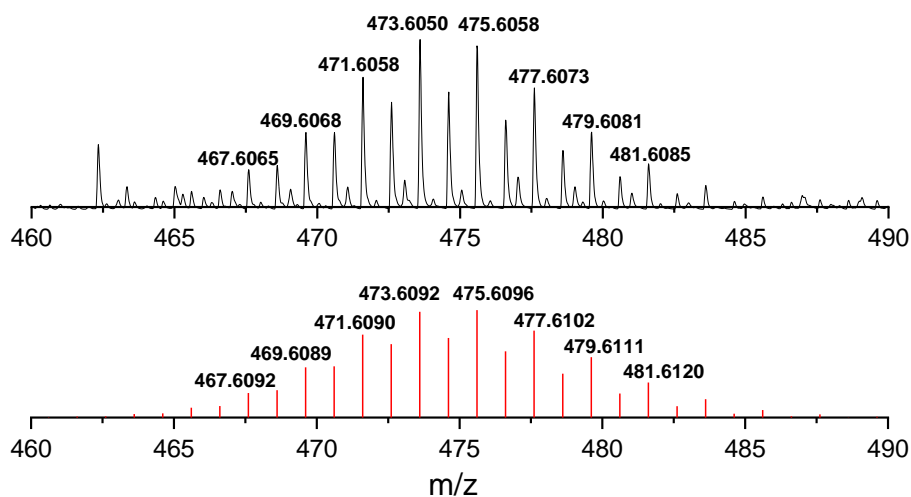
m/z

Figure S7. Measured (top) and simulated (bottom) spectrum of the fragment $\{[Sn_4(ZnMes)_2]\}^-$.

7
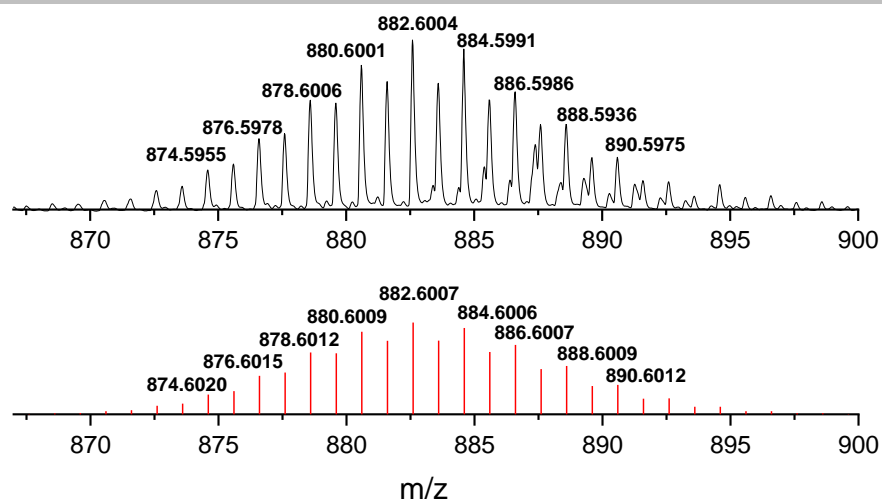
Figure S8. Measured (top) and simulated (bottom) spectrum of the fragment {[KSn$_4$(ZnMes)$_2$]}$^-$.

Figure S9. Measured (top) and simulated (bottom) spectrum of the fragment {[Sn$_4$]}$^-$.

Section 4: Energy Dispersive X-ray (EDX) Spectroscopic Analysis

The EDX shows the atom% values of K: Zn: Sn= 8.6 %:12.5 %:78.9 % (Figure S10) compared with the theoretical values of K$_8$Zn$_4$Sn$_{16}$: 12.6 %:10.6 %:76.8 %. A deviation of the amount of K is observed in the EDX characterization, which may be caused by the irregular surfaces of the crystals after exposing in air.
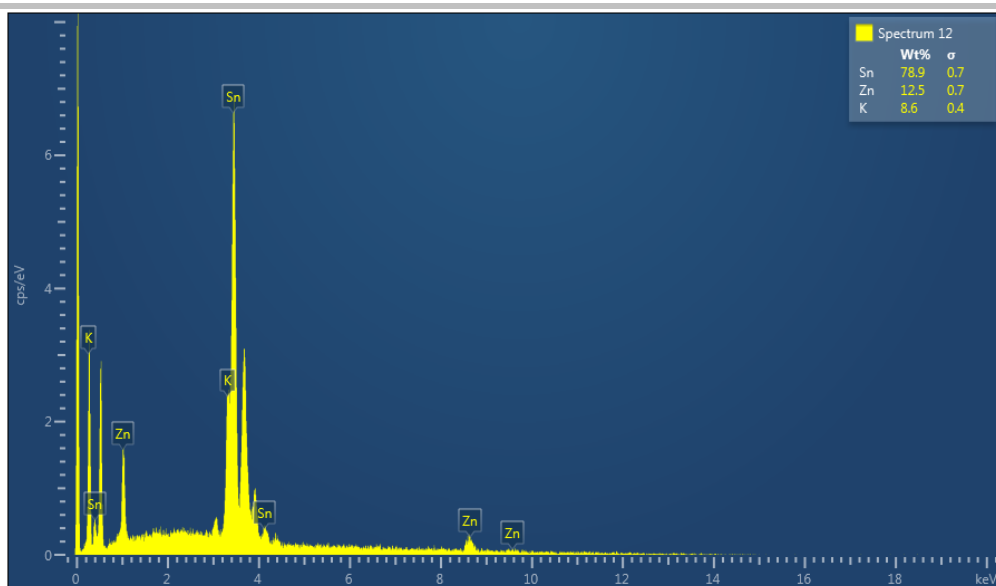
Figure S10. EDX analysis of **1** (K, Zn, Sn).
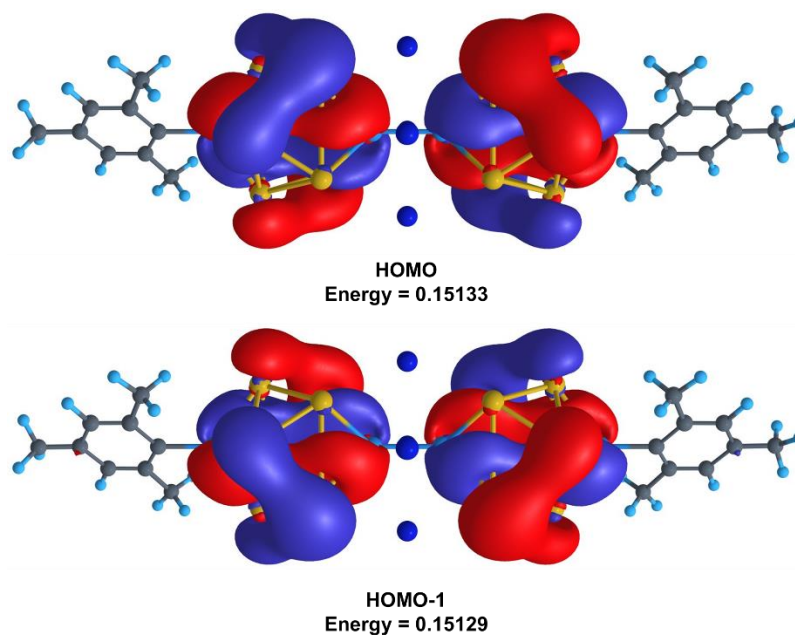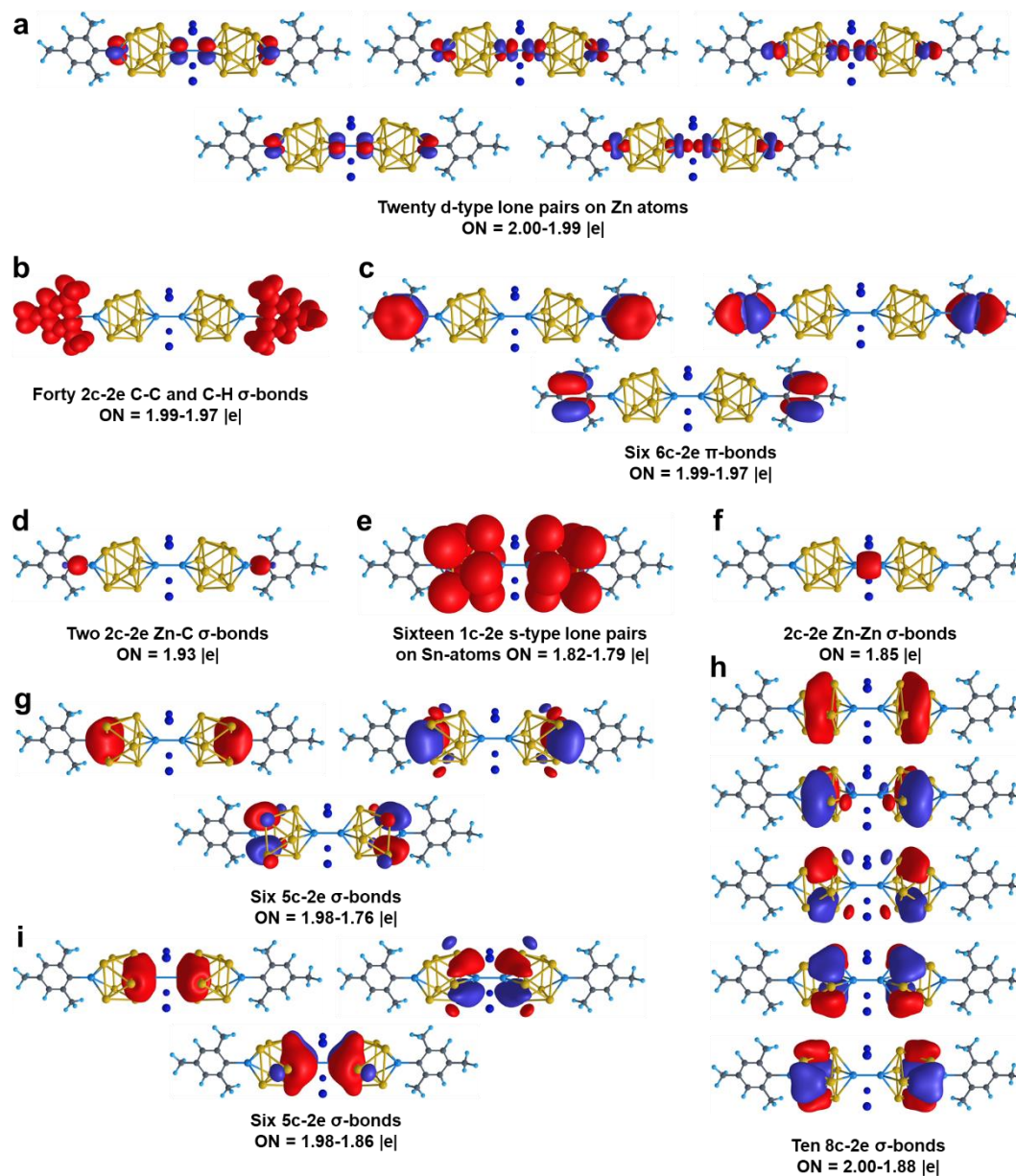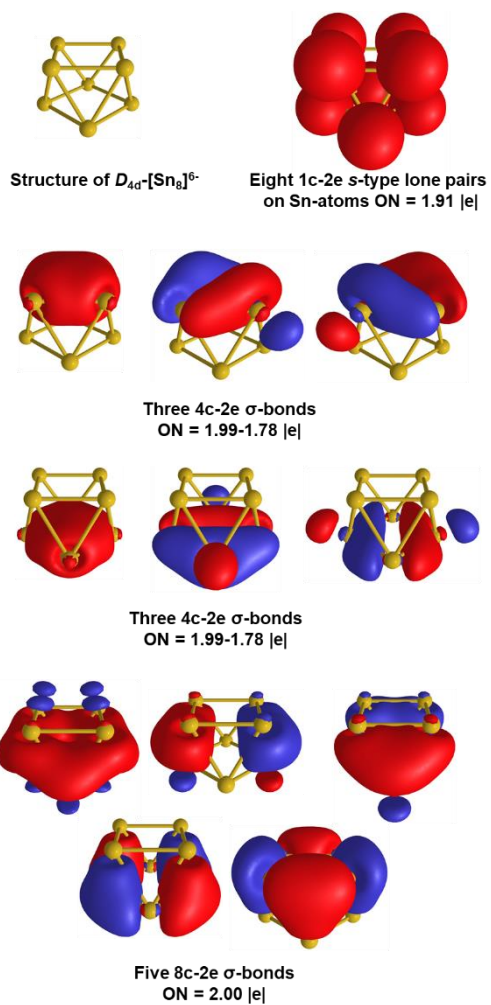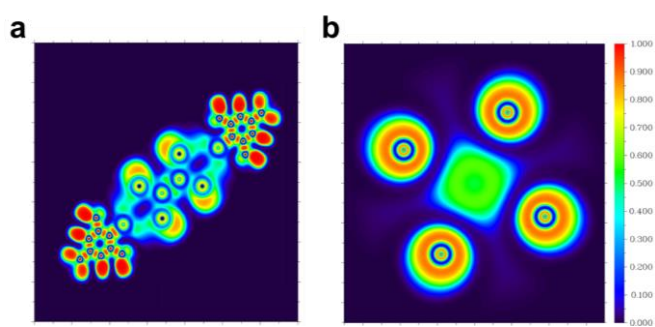
Section 5: Computational Details

HOMO
Energy = 0.15133

HOMO-1
Energy = 0.15129

Figure S11. Plots of HOMO/HOMO-1 molecular orbitals and their energy (Hartree) for $\{[K_2ZnSn_8(ZnMes)]_2\}^{4-}$ cluster.

a

Twenty d-type lone pairs on Zn atoms
ON = 2.00-1.99 |e|

b

Forty 2c-2e C-C and C-H σ-bonds
ON = 1.99-1.97 |e|

c

Six 6c-2e π-bonds
ON = 1.99-1.97 |e|

d

Two 2c-2e Zn-C σ-bonds
ON = 1.93 |e|

e

Sixteen 1c-2e s-type lone pairs
on Sn-atoms ON = 1.82-1.79 |e|

f

2c-2e Zn-Zn σ-bonds
ON = 1.85 |e|

g

Six 5c-2e σ-bonds
ON = 1.98-1.76 |e|

h

Ten 8c-2e σ-bonds
ON = 2.00-1.88 |e|

i

Six 5c-2e σ-bonds
ON = 1.98-1.86 |e|

Figure S12. The complete chemical bonding pattern of {[K$_2$ZnSn$_8$(ZnMes)]$_2$}$^{4-}$ cluster.

Structure of D_{4d}-[Sn_8]$^{6-}$

Eight 1c-2e *s*-type lone pairs on Sn-atoms ON = 1.91 |e|

Three 4c-2e σ-bonds ON = 1.99-1.78 |e|

Three 4c-2e σ-bonds ON = 1.99-1.78 |e|

Five 8c-2e σ-bonds ON = 2.00 |e|

Figure S13. The complete chemical bonding pattern of [Sn_8]$^{6-}$ cluster.

Figure S14. ELF plots of [$K_4Zn_4Sn_{16}$]$^{4-}$ {[$K_2ZnSn_8(ZnMes)$]$_2$}$^{4-}$ cluster. a: plot is built in the plane of C_6 rings; b: plot is built in the plane of K_4 square.
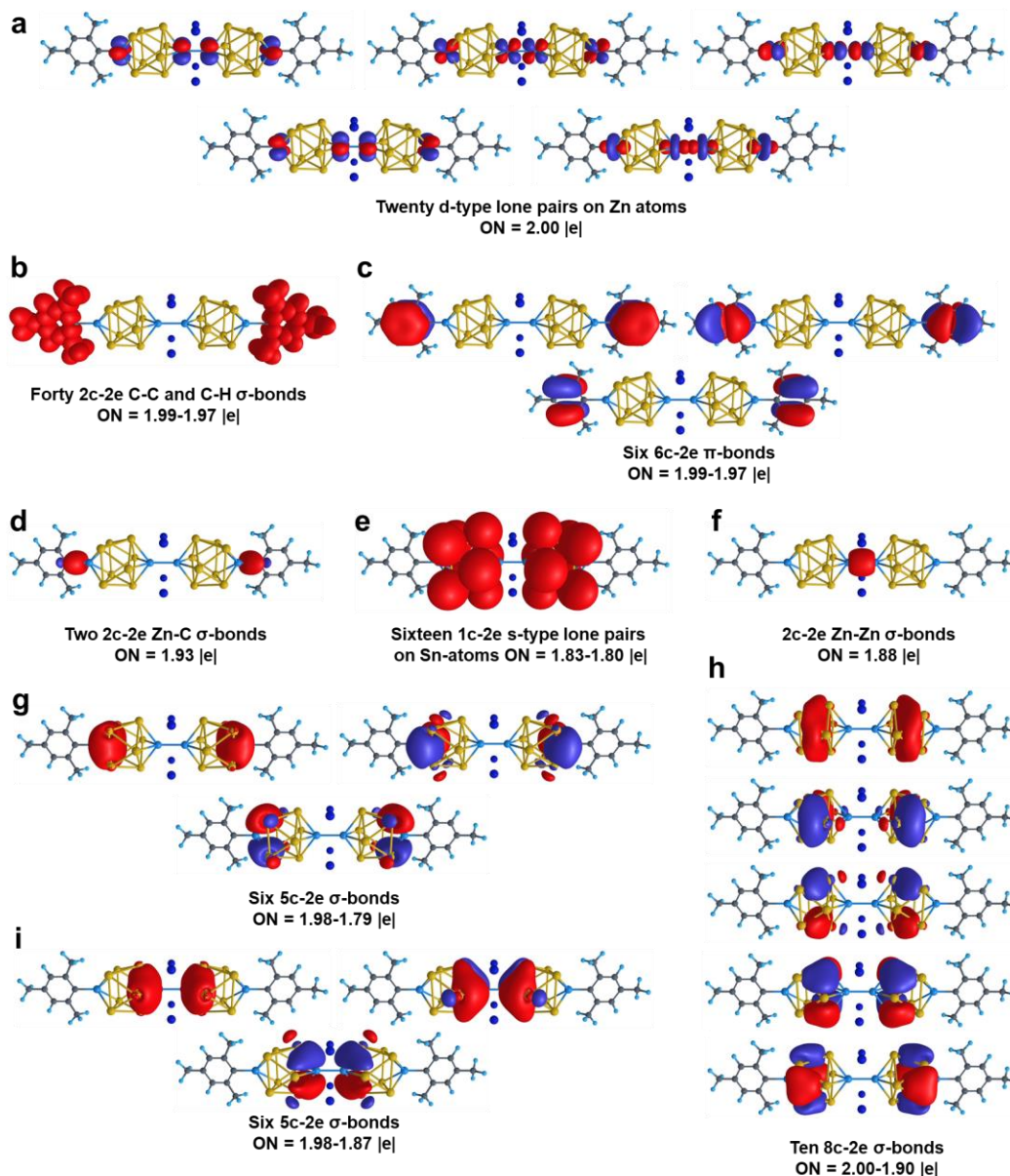
Figure S15. The complete chemical bonding pattern of $\{[K_2ZnSn_8(ZnMes)]_2\}^{4-}$ cluster calculated at CAM-B3LYP/def3tzvp level of theory.

Comparison of the chemical bonding of $\{[K_2ZnSn_8(ZnMes)]_2\}^{4-}$ cluster with $ArZn(\mu-H)_2ZnAr$ species.

The slightly elongated Zn-Zn bond can be a consequence of electrostatic repulsion between two negatively charged clusters. Such elongation makes the Zn-Zn in the title cluster in the range of Zn-Zn distances in the hydride species with $Zn(\mu-H)_2Zn$ fragment. To illustrate that the chemical bonding between Zn-atoms in the case of hydride species is completely different from our case let us consider an artificial model $MesZn(\mu-H)_2ZnMes$ complex. The chemical bonding of $Zn(\mu-H)_2Zn$ fragment consists of two 3c-2e Zn-H-Zn bonds (with a high contribution of H-atom), and no true 2c-2e Zn-Zn bond is present. Zn-atoms donate their electrons to hydrogen-atom, so the H-atoms are in -1 formal oxidation state and the oxidation state of Zn is formally +2 which agrees with calculated natural charges. The ELF analysis showing low localization of electrons between two Zn-atoms; QTAIM analysis is showing no bond critical points between two Zn-atoms. Thus, the chemical bonding of the hydride species is different from the one that was presented in the manuscript and cannot be described as Zn-Zn 2c-2e covalent interaction.
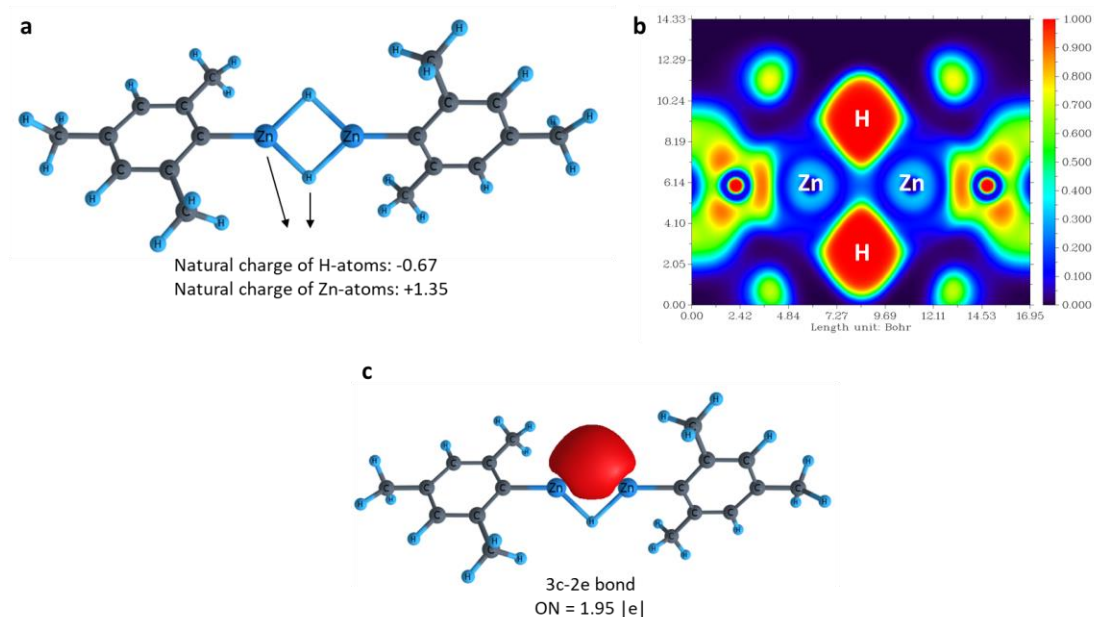
Figure S16. a) Natural charges of Zn and H atoms in MesZn(μ-H)₂ZnMes complex. b) ELF plot of of Zn(μ-H)₂Zn f ragment in in MesZn(μ-H)₂ZnMes complex. c) The 3c-2e bonding element of Zn(μ-H)₂Zn f ragment in MesZn(μ-H)₂ZnMes complex.

Table S2. Cartesian coordinates of optimized clusters.

$[K_4Zn_4Sn_{16}]^{4-}$	PBE0/def2tzvp, NIMAG = 0		
	50	-0.764401000	2.967773000	2.121053000
	50	0.963057000	5.369280000	2.054835000
	50	-2.050823000	5.369924000	0.968094000
	50	-2.123224000	-2.975309000	-0.766686000
	50	-2.123497000	2.976611000	-0.764609000
	50	2.051780000	5.369853000	-0.964328000
	50	-0.962040000	5.370880000	-2.051264000
	50	-0.764362000	-2.968830000	2.118718000
	30	0.000630000	-1.279106000	-0.000605000
	30	0.000795000	7.042931000	0.002363000
	19	1.319824000	-0.000901000	2.807113000
	19	-2.807036000	-0.000872000	1.320039000
	6	-0.407342000	11.240209000	1.117128000
	1	-0.727489000	11.778308000	2.009968000
	6	-0.002085000	9.101085000	0.001813000
	6	-0.410996000	9.844059000	1.126493000
	6	0.409802000	9.844567000	-1.121518000
	6	0.871766000	9.144222000	-2.367024000
	1	1.726444000	8.493164000	-2.158469000
	1	1.154477000	9.857725000	-3.149032000
	1	0.091927000	8.483432000	-2.758227000
	6	-0.003563000	11.961614000	0.001860000
	6	0.406547000	11.240656000	-1.111443000

13

1	0.737246000	11.779089000	-2.000235000
6	-0.860109000	9.143218000	2.376418000
1	-1.145615000	9.856421000	3.157686000
1	-0.072849000	8.490286000	2.765953000
1	-1.710042000	8.484223000	2.173470000
6	-0.040991000	13.463399000	-0.011596000
1	-1.005472000	13.846693000	-0.370131000
1	0.732178000	13.875033000	-0.668478000
1	0.115143000	13.874277000	0.991129000
50	0.764401000	-2.967773000	-2.121053000
50	-0.963057000	-5.369280000	-2.054835000
50	2.050823000	-5.369924000	-0.968094000
50	2.123224000	2.975309000	0.766686000
50	2.123497000	-2.976611000	0.764609000
50	-2.051780000	-5.369853000	0.964328000
50	0.962040000	-5.370880000	2.051264000
50	0.764362000	2.968830000	-2.118718000
30	-0.000630000	1.279106000	0.000605000
30	-0.000795000	-7.042931000	-0.002363000
19	-1.319824000	0.000901000	-2.807113000
19	2.807036000	0.000872000	-1.320039000
6	0.407342000	-11.240209000	-1.117128000
1	0.727489000	-11.778308000	-2.009968000
6	0.002085000	-9.101085000	-0.001813000
6	0.410996000	-9.844059000	-1.126493000
6	-0.409802000	-9.844567000	1.121518000
6	-0.871766000	-9.144222000	2.367024000
1	-1.726444000	-8.493164000	2.158469000
1	-1.154477000	-9.857725000	3.149032000
1	-0.091927000	-8.483432000	2.758227000
6	0.003563000	-11.961614000	-0.001860000
6	-0.406547000	-11.240656000	1.111443000
1	-0.737246000	-11.779089000	2.000235000
6	0.860109000	-9.143218000	-2.376418000
1	1.145615000	-9.856421000	-3.157686000
1	0.072849000	-8.490286000	-2.765953000
1	1.710042000	-8.484223000	-2.173470000
6	0.040991000	-13.463399000	0.011596000
1	1.005472000	-13.846693000	0.370131000
1	-0.732178000	-13.875033000	0.668478000
1	-0.115143000	-13.874277000	-0.991129000
[K$_4$Zn$_4$Sn$_{16}$]$^{4-}$	CAM-B3LYP/def2tzvp, NIMAG = 0		
50	-0.766291000	2.959655000	2.117151000
50	0.965191000	5.349716000	2.062136000
50	-2.058925000	5.350844000	0.966569000
50	-2.119085000	-2.965758000	-0.768668000
50	-2.118740000	2.967496000	-0.766572000
50	2.061001000	5.350460000	-0.962649000
50	-0.963051000	5.351622000	-2.058356000
50	-0.766925000	-2.960696000	2.114798000
30	0.000520000	-1.272705000	-0.000552000

14

30	0.001516000	6.994156000	0.002510000
19	1.309238000	-0.000997000	2.795236000
19	-2.795126000	-0.000639000	1.309606000
6	-0.405102000	11.202586000	1.114177000
1	-0.724006000	11.738680000	2.005568000
6	-0.001028000	9.063007000	0.002122000
6	-0.407892000	9.808680000	1.123647000
6	0.408029000	9.809241000	-1.118296000
6	0.871545000	9.117579000	-2.372468000
1	1.728319000	8.472323000	-2.172763000
1	1.150556000	9.839533000	-3.145282000
1	0.094590000	8.463485000	-2.770922000
6	-0.003910000	11.923060000	0.001741000
6	0.403939000	11.203093000	-1.108649000
1	0.732629000	11.739594000	-1.996241000
6	-0.858827000	9.116451000	2.382090000
1	-1.140253000	9.838063000	3.154348000
1	-0.074646000	8.469775000	2.778528000
1	-1.711190000	8.463681000	2.188066000
6	-0.042312000	13.427715000	-0.011974000
1	-1.006387000	13.807734000	-0.367388000
1	0.727898000	13.838139000	-0.669504000
1	0.116552000	13.837481000	0.988438000
50	0.766291000	-2.959655000	-2.117151000
50	-0.965191000	-5.349716000	-2.062136000
50	2.058925000	-5.350844000	-0.966569000
50	2.119085000	2.965758000	0.768668000
50	2.118740000	-2.967496000	0.766572000
50	-2.061001000	-5.350460000	0.962649000
50	0.963051000	-5.351622000	2.058356000
50	0.766925000	2.960696000	-2.114798000
30	-0.000520000	1.272705000	0.000552000
30	-0.001516000	-6.994156000	-0.002510000
19	-1.309238000	0.000997000	-2.795236000
19	2.795126000	0.000639000	-1.309606000
6	0.405102000	-11.202586000	-1.114177000
1	0.724006000	-11.738680000	-2.005568000
6	0.001028000	-9.063007000	-0.002122000
6	0.407892000	-9.808680000	-1.123647000
6	-0.408029000	-9.809241000	1.118296000
6	-0.871545000	-9.117579000	2.372468000
1	-1.728319000	-8.472323000	2.172763000
1	-1.150556000	-9.839533000	3.145282000
1	-0.094590000	-8.463485000	2.770922000
6	0.003910000	-11.923060000	-0.001741000
6	-0.403939000	-11.203093000	1.108649000
1	-0.732629000	-11.739594000	1.996241000
6	0.858827000	-9.116451000	-2.382090000
1	1.140253000	-9.838063000	-3.154348000
1	0.074646000	-8.469775000	-2.778528000
1	1.711190000	-8.463681000	-2.188066000

	6	0.042312000	-13.427715000	0.011974000
	1	1.006387000	-13.807734000	0.367388000
	1	-0.727898000	-13.838139000	0.669504000
	1	-0.116552000	-13.837481000	-0.988438000
$[Sn_8]^{6-}$	PBE0/def2tzvp, NIMAG = 0			
	50	0.000000000	2.202847000	1.317876000
	50	-2.202847000	0.000000000	1.317876000
	50	2.202847000	0.000000000	1.317876000
	50	1.557648000	1.557648000	-1.317876000
	50	1.557648000	-1.557648000	-1.317876000
	50	0.000000000	-2.202847000	1.317876000
	50	-1.557648000	1.557648000	-1.317876000
	50	-1.557648000	-1.557648000	-1.317876000

Table S3. Calculated charges [a.u.] of selected atoms of . $[K_4Zn_4Sn_{16}]^{4-}$ cluster. Indices of atoms are in accordance with Table S2.

Atom	NAO - charge	QTAIM - charge	CM5 - charge
Sn 1	-0.75595	-0.49573	-0.32854
Sn 2	-0.4255	-0.26183	-0.2698
Sn 3	-0.42581	-0.28451	-0.26969
Sn 4	-0.74485	-0.53177	-0.32737
Sn 5	-0.74446	-0.53245	-0.3272
Sn 6	-0.42564	-0.21181	-0.26961
Sn 7	-0.42564	-0.14614	-0.26987
Sn 8	-0.75612	-0.49624	-0.32862
Zn 9	0.60058	-0.28389	0.01863
Zn 10	1.23458	0.13499	0.250381
K 11	0.85058	0.785614	0.362216
K 12	0.85058	0.78288	0.362209
Sn 33	-0.75595	-0.45405	-0.32854
Sn 34	-0.4255	-0.1472	-0.2698
Sn 35	-0.42581	-0.21042	-0.26969
Sn 36	-0.74485	-0.55949	-0.32737
Sn 37	-0.74446	-0.56008	-0.3272
Sn 38	-0.42564	-0.28477	-0.26961
Sn 39	-0.42564	-0.26195	-0.26987
Sn 40	-0.75612	-0.45459	-0.32862

16

Zn 41	0.60058	-0.284	0.01863
Zn 42	1.23458	0.145769	0.250381
K 43	0.85058	0.791229	0.362216
K 44	0.85058	0.785809	0.362209

References

[1] D. J. J. Dunsford *et al.*, *Angew. Chem. Int. Ed.* **2015**, 127, 5780-5784.
[2] G. M. Sheldrick, *Acta Crystallogr. Sect. A: Found. Adv.* **2015**, 71, 3-8.
[3] O. V. Dolomanov, L. J. Bourhis, R. J. Gildea, J. A. K. Howard, H. Puschmann, *J. Appl. Crystallogr.* **2009**, 42, 339-341.
[4] A. L. Spek, *Acta Crystallogr., Sect. D: Biol. Crystallogr.* **2009**, 65, 148-155.
[5] A. L. Spek, *Acta Crystallogr. Sect. C Cryst. Struct. Commun.* **2015**, 71, 9-18.
[6] Y. Grin, M. Baitinger, R. Kniep, H. G. v. Schnering, *Z. Kristallogr. NCS* **1999**, 214, 453-454.
[7] E. D. Glendening, J, K. Badenhoop, A. E. Reed, J. E. Carpenter, J. A. Bohmann, C. M. Morales, P. Karafiloglou, C. R. Landis, and F. Weinhold, *NBO 7.0.* Theoretical Chemistry Institute, University of Wisconsin, Madison, **2018**.

Author Contributions